

Beyond Transcription: Mechanistic Interpretability in ASR

Neta Glazer, Yael Segal-Feldman, Hilit Segev, Aviv Shamsian, Asaf Buchnick, Gill Hetz, Ethan Fetaya, Joseph Keshet, Aviv Navon

aiOla Research
neta.glazer@aiola.com

Abstract

Interpretability methods have recently gained significant attention, particularly in the context of large language models, enabling insights into linguistic representations, error detection, and model behaviors such as hallucinations and repetitions. However, these techniques remain underexplored in automatic speech recognition (ASR), despite their potential to advance both the performance and interpretability of ASR systems. In this work, we adapt and systematically apply established interpretability methods such as logit lens, linear probing, and activation patching, to examine how acoustic and semantic information evolves across layers in ASR systems. Our experiments reveal previously unknown internal dynamics, including specific encoder-decoder interactions responsible for repetition hallucinations and semantic biases encoded deep within acoustic representations. These insights demonstrate the benefits of extending and applying interpretability techniques to speech recognition, opening promising directions for future research on improving model transparency and robustness.

1 Introduction

Automatic Speech Recognition has advanced significantly in recent years, largely driven by powerful neural architectures trained on extensive speech datasets (Radford et al. 2023; Chu et al. 2023). Modern ASR systems commonly utilize encoder-decoder transformer architectures, facilitating robust recognition across diverse languages, accents, and acoustic conditions (Radford et al. 2023; Chu et al. 2024; Abouelenin et al. 2025). Recently, architectural approaches have diverged, with some models adopting Large Audio-Language Models (LALMs) that integrate pretrained language models (Tang et al. 2023; Das et al. 2024; Abouelenin et al. 2025), such as Qwen2-Audio (Chu et al. 2023, 2024), while others continue to rely on transformers specifically trained for speech, such as Whisper (Radford et al. 2023).

In parallel, interpretability has become a central research focus in large language model (LLMs) (Brown et al. 2020; Touvron et al. 2023; Team 2024), with growing efforts to understand how these models represent information and produce decisions (Luo and Specia 2024).

Techniques linear probing (Belinkov 2022; McKenzie et al. 2025), logit lens (Geva et al. 2022; nostalgebraist 2020), and activation patching (Meng et al. 2022; Wang et al. 2022) allow researchers to reverse-engineer internal model behavior, revealing the structure of linguistic representations and tracing the origins of specific outputs. These tools have proven crucial in diagnosing failure modes like hallucinations and reasoning errors, and have contributed to improving model safety and reliability.

In this work, we take a first step toward bridging the interpretability gap in ASR. We examine the internal behavior and dynamics of modern ASR and Large Audio-Language Models to understand the mechanisms behind key error phenomena such as hallucinations, repetition loops, and contextually biased outputs. In addition, we trace how predictions evolve across layers, identify which components drive specific decoding behaviors, and reveal how contextual expectations compete with acoustic evidence. Beyond error analysis, we investigate the rich representations these models encode, from quality prediction signals embedded in decoder states to localized attention mechanisms that control model failures.

To better understand these phenomena, we systematically adapt interpretability techniques to reveal the internal mechanisms of these models. We find that acoustic and semantic attributes are linearly decoded in the encoder layers, with clearer separation in upper layers. We discover that hallucination-related signals are strongly expressed in the decoder’s residual stream, enabling an accurate real-time quality prediction. Furthermore, we identify the specific mechanisms responsible for repetitions, revealing which components control these failure modes. Additionally, we show that contextual bias emerges within the encoder itself and can override acoustic evidence, challenging assumptions about encoder-decoder role separation.

This work takes a step toward systematically understanding of the internal dynamics and decision-making processes of speech recognition models, opening new directions for improving their reliability and performance.

2 Related Work

A substantial amount of research has focused on understanding how LLMs process and represent information (Räuker et al. 2023), ranging from identifying specific circuits responsible for particular tasks (Hanna, Liu, and Variengien 2023; Goldowsky-Dill et al. 2023) to exploring how the model “thinks” (Schut, Gal, and Farquhar 2025) and which components responsible for repetitions (Yona et al. 2025; Barbero et al. 2024). The methods used to understand the model are varied. For example, the logit lens and its improved variant Tuned Lens track how token predictions evolve across layers, providing a layer-wise view of model behavior (nostalgia 2020; Geva et al. 2022; Belrose et al. 2023). Complementary approaches such as linear probing test whether models encode features like syntax or factual knowledge in directions recoverable by simple classifiers (Belinkov 2022; McKenzie et al. 2025; Hernandez et al. 2023). Building on this, activation patching and causal tracing explore the causal role of specific hidden states by swapping or ablating them to observe changes in outputs (Meng et al. 2022; Heimersheim and Nanda 2024). More recently, attribution patching has extended these ideas to finer-grained structures by using gradients to pinpoint influential neurons (Syed, Rager, and Conmy 2023; Nanda 2023; Kramář et al. 2024). Collectively, these methods represent diverse attempts to interpret how LLMs operate internally.

Several studies have examined the internal representations learned by the Whisper model. These studies show that the Whisper encoder captures noise-related features, speaker identity, and emotional content (Gong et al. 2023; Upadhyay, Busso, and Lee 2024; Zhao et al. 2024), while the decoder also encodes speaker traits and reacts to language shifts (Berns, Vaessen, and van Leeuwen 2023). However, these works did not target model interpretability. A blog post by Reid (2023) offers the first large-scale interpretability analysis, revealing that encoder neurons align with human-interpretable phoneme patterns, and that the decoder mainly acts as a weak language model. Other works extend this line of inquiry in different directions: Lioubashevski et al. (2024) show that decoder based LLM including Whisper first stabilize on the top-ranking token, then successively the next highest-ranked tokens; Ballier et al. (2024) apply probing methods to analyze calibration curves across multiple languages; and Barański et al. (2025) investigate hallucinations over non-speech segments, aiming to catalog frequently occurring hallucinations rather than localizing them within model components. Yang, Huang, and Lee (2024) explores the influence of text prompts on Whisper’s outputs.

3 Method

In this section, we present the interpretability techniques employed in our study. Since these methods were originally developed for LLMs or vision models, we describe the adaptations required to apply them effec-

tively in the ASR setting. We begin by introducing the notation used throughout.

3.1 Preliminaries and Notation

We consider encoder-decoder ASR models that generate a sequence of tokens $\mathbf{y} = (y_1, \dots, y_T)$ from input audio \mathbf{x} , using a Transformer encoder and decoder (Vaswani et al. 2017). Let L_e and L_d denote the number of encoder and decoder layers, respectively, and d the hidden dimension.

The encoder processes audio into a sequence of hidden vectors. We denote by $\mathbf{h}^{l_e} \in \mathbb{R}^{F \times d}$ the encoder representation at layer $l_e \in \{1, \dots, L_e\}$, where F is the number of audio frame representations after feature extraction. We use $\mathbf{h}_\tau^{l_e} \in \mathbb{R}^d$ to refer to the representation at position $\tau \in \{1, \dots, F\}$ and by $\mathbf{h}_t^{l_d} \in \mathbb{R}^d$ the decoder hidden state at layer l_d and token position t . The decoder output is projected to vocabulary logits using the unembedding matrix $E \in \mathbb{R}^{|\mathcal{V}| \times d}$ using

$$\mathbf{z}_t^{l_d} = E \cdot \mathbf{r}_t^{l_d} \in \mathbb{R}^{|\mathcal{V}|}.$$

Here $\mathbf{r}_t^{l_d} \in \mathbb{R}^d$ is the residual stream, which captures the decoder’s intermediate representation after layer normalization but before output projection.

3.2 Interpretability Methods

Logit Lens. The logit lens (Geva et al. 2022) provides a layer-by-layer view of how the model’s predictions evolve during decoding. At each decoding step t , we take the residual stream $\mathbf{r}_t^{l_d}$ from each decoder layer l_d , and project it to the vocabulary space using the unembedding matrix E , to produce the logits vector $\mathbf{z}_t^{l_d}$. We extract the top- k tokens from each $\mathbf{z}_t^{l_d}$ to analyze how predictions develop across layers. To quantify this process, we follow Geva et al. (2022); Lioubashevski et al. (2024), and define the *saturation layer* of a token t as the earliest decoder layer whose top-1 prediction matches the final output and remains stable:

$$l_t^* = \min \left\{ l_d : \arg \max \mathbf{z}_t^{l_d} = \arg \max \mathbf{z}_t^{L_d} \right\}.$$

This provides insight into when the model effectively commits to a prediction.

Activation Probing. Probing tests whether specific attributes are encoded in a model’s hidden representations (Belinkov 2022). We use linear probes: simple classifiers trained on frozen activations $\mathbf{h} \in \mathbb{R}^d$ to predict a label,

$$\mathcal{P}(\mathbf{h}) = W\mathbf{h} + b,$$

where $W \in \mathbb{R}^{k \times d}$, $b \in \mathbb{R}^k$ are trained using cross-entropy or regression loss. High accuracy suggests that the attribute is linearly decodable from the representation (Hernandez et al. 2023).

For decoder, we probe token-level hidden states (typically at the final position). In the encoder, where representations are aligned with audio frames, we average across time to produce a fixed-length vector. Probes may be reused at inference to monitor internal structure with minimal overhead (McKenzie et al. 2025).

Intervention-Based Analysis. Causal intervention methods study why a model produces a particular output by modifying its internal activations and observing the effect on predictions. If modifying a component changes the output, that component is said to play a causal role in the behavior. This idea underlies recent work on factual editing and mechanism tracing in LLMs and vision models (Meng et al. 2022; Wang et al. 2022; Ben Melech Stan et al. 2024; Haklay et al. 2025). We adapt two standard interventions, component patching and ablation, to analyze Whisper and Qwen2-Audio.

Component patching. In this technique, we run the model on two inputs: a target input and a reference input. During the forward pass on the target input, we replace the activation of a selected component with the one recorded from the reference input. Formally, let $\mathbf{a}_C^{\text{orig}}$ be the activation at component C when running the original input \mathbf{x}_{orig} , and let $\mathbf{a}_C^{\text{ref}}$ be the corresponding activation from a reference input \mathbf{x}_{ref} . We compute a patched activation as:

$$\tilde{\mathbf{a}}_C = (1 - \alpha) \mathbf{a}_C^{\text{orig}} + \alpha \mathbf{a}_C^{\text{ref}}, \quad \alpha \in \mathbb{R}_+.$$

In our experiments, we use white noise as the reference input, which serves to disrupt the natural computation. This helps reveal components that are critical for maintaining acoustic fidelity or contextual bias.

Ablation. Ablation tests whether a component is necessary for a model behavior by removing its contribution during inference (Vig et al. 2020). This is done by zeroing out the activation at component C , $\tilde{\mathbf{a}}_C = \mathbf{0}$, and observing the change in output. If the prediction is degraded or altered, we interpret this as evidence that C is important for producing the original behavior.

Intervention Scope. We apply interventions on both encoder and decoder layers, targeting sub-modules such as cross attention, self-attention and feed-forward blocks. In attention layers, we also intervene at the head level.

Encoder Lens. We introduce Encoder Lens, a method for analyzing intermediate encoder representations in ASR models. Inspired by the Diffusion Lens framework for interpreting text encoders in text-to-image models (Toker et al. 2024), our goal is to examine how representations evolve across encoder layers in encoder-decoder ASR systems.

Given an input audio signal \mathbf{x} , the encoder produces a sequence of hidden vectors $\mathbf{h}_\tau^{l_e} \in \mathbb{R}^d$ at each layer $l_e \in \{1, \dots, L_e\}$. For each layer, we extract the full representation $\mathbf{h}_e^{l_e} \in \mathbb{R}^{F \times d}$, apply the model’s final encoder layer normalization, and pass it directly into the decoder. As in Toker et al. (2024), we find that applying the final layer normalization is crucial. Without it, the decoder struggles to produce coherent or grammatical output. This process constructs a textual representation for each encoder layer, which we further analyze in Section 3.2.

4 Experiments

Our experiments focus on two state-of-the-art ASR systems with distinct architectural designs:

Whisper. We use whisper-large-v3 (Radford et al. 2023), an encoder-decoder model designed for multilingual speech-to-text and speech translation tasks. It features a 32-layer audio encoder and a 32-layer text decoder, trained jointly on large-scale paired audio-text datasets. The model has $\sim 1.5\text{B}$ parameters in total.

Qwen2-Audio. We use Qwen2-Audio-7B-Instruct (Chu et al. 2024), a Large Audio Language Model with $\sim 8.2\text{B}$ parameters. It combines a frozen whisper-large-v3 encoder with a Qwen2.5-7B decoder, trained for multimodal instruction following including audio transcription. The encoder output is prepended to the decoder input as a prefix, enabling the model to handle both spoken and textual instructions.

4.1 Probing for Transcription Enrichment

While ASR models are trained to produce transcriptions, both their encoder and decoder layers capture a broad range of information beyond the spoken words. By training simple probes on internal activations (Section 3.2), we can reveal that specific layers encode various attributes despite these properties not being part of the model’s supervision.

Once such attributes are encoded, they remain accessible throughout the forward pass. This means that a single transcription run implicitly generates a much richer representation, capturing both acoustic and contextual information. The examples shown here demonstrate just a few of the many properties that can be extracted from intermediate layers across the model. Full layerwise results and training details appear in the Appendix.

Speaker Gender. We examine whether speaker gender is encoded in the shared Whisper-large-v3 encoder used by both Whisper and Qwen2-Audio. We train linear probes on 2,000 labeled examples from LibriSpeech (Panayotov et al. 2015), and evaluate on 500 samples from the test-clean split. We apply probes to each encoder layer individually. The best performance is observed at layer 25, achieving 94.6% accuracy, indicating strong linear decodability of gender features in deeper layers. For comparison, asking Qwen2-Audio to determine speaker gender based on its textual outputs yields only 87.8% accuracy. This demonstrates that the model knows more than it explicitly shows in its outputs, a phenomenon that was also reported in LLMs (Orgad et al. 2024), and highlights the advantage of probing internal representations.

Clean vs. Noisy Environment. Next, we investigate whether noisy environment is reflected in the Whisper encoder hidden representation. We train linear probes using examples from the dev-clean (speech recorded in clean conditions) and dev-other (noisy or challenging conditions) splits of LibriSpeech, and test on the corresponding test-clean and test-other

splits. Probes are applied to individual encoder layers. The best performance is observed at layer 27, reaching 90.0% accuracy, indicating that the encoder effectively separates clean from noisy speech.

Accents Finally, we assess whether speaker accent is reflected in the Whisper encoder representations by performing multi-class classification over accent categories. Using the English Accent Dataset (Wang), we select four accent groups: New Zealand, Welsh Valleys, South African, and Indian. We train linear probes on 2,400 samples (600 per class), and evaluate on 337 test samples. The best performance is observed at encoder layer 22, reaching 97.0% average accuracy. Class-wise accuracies are also high: 95.7% for Indian, 95.8% for New Zealand, 96.1% for South African, and 99.2% for Welsh Valleys. This result suggests that accent information is linearly decodable from intermediate audio representations.

4.2 Probing for Hallucination Monitoring

In this section, we investigate whether model hallucinations can be predicted from internal decoder representations. First, we examine whether hallucinations can be predicted from the residual stream. Second, we probe the hidden representations to identify non-speech content, with a focus on hallucinations caused by misinterpreting silence or background noise inputs.

Hallucination Prediction from Decoder Residual Stream. Here, we ask whether hallucinations can be predicted in advance by examining the model’s internal state. Inspired by findings in the LLM literature (O’Neill et al. 2025), we test this hypothesis by linearly probing the ASR decoder’s residual stream at the final token position (`<eos>` token) across all layers.

To that end, we pose a binary classification task to differentiate between samples with zero and high word error rate (WER). We transcribe the test-clean subset of LibriSpeech (Panayotov et al. 2015) and CommonVoice 16.1 (Ardila et al. 2020) datasets using each target model, then select 150 samples with zero WER and the 200 samples with highest WER values, creating a 400-sample dataset split 70%-30% into training and test sets. This creates a challenging task where each model must distinguish between its own high-quality and severely degraded transcriptions.

We verified that the text length distributions are identical between the low and high WER groups, ensuring that classification performance reflects transcription quality differences rather than length biases.

We train linear probes on the final token’s residual stream representation to distinguish between high-quality transcriptions and hallucinations. Surprisingly, the results show that hallucinations can be accurately identified by linear probing the decoder’s residual stream, with maximum accuracy of 93.4% at layer 22. This suggests that Whisper encodes quality-related signals deep in the decoder at the completion of text generation, enabling lightweight hallucination prediction di-

rectly from internal activations. We repeat the experiment on the Common Voice dataset and achieve 88.1% accuracy at layer 22, confirming that hallucination-related signals are consistently embedded in the residual stream across domains.

Next, we conduct the same linear probing experiments with Qwen2-Audio. On the LibriSpeech dataset, the peak accuracy achieved by the linear probe was 70.2% at layer 22. For the Common Voice dataset, the probe reached an accuracy of 83.6%, also at layer 22, suggesting consistent architectural patterns for quality encoding across different ASR models. Detailed results across all layers and additional experimental details are provided in the Appendix.

Speech vs. Non-Speech for Non-Speech Hallucinations. Recent studies show that ASR models, such as Whisper, may hallucinate by generating grammatically correct transcriptions for non-speech audio inputs (Barański et al. 2025; Frieske and Shi 2024).

In this section, we investigate whether internal activations alone can reliably distinguish speech from non-speech inputs, enabling enriched transcript metadata during inference. Such capability would allow systems to flag potentially hallucinated outputs when processing ambiguous audio streams.

To evaluate this, we construct a balanced binary classification dataset of 800 samples: 400 speech samples from LibriSpeech (Panayotov et al. 2015), CommonVoice (Ardila et al. 2020), and MLS (Pratap et al. 2020), and 400 non-speech samples from MUSAN (Snyder, Chen, and Povey 2015), FSD50K (Fonseca et al. 2021), AudioCaps (Kim et al. 2019), and generated white noise, encompassing diverse acoustic environments and sound events. We focus specifically on the more challenging cases where non-speech audios are transcribed into coherent words.

We probe the decoder’s hidden states using linear classifiers trained on the final token representation at each layer. The results reveal perfect classification performance (100% accuracy) from layers 10–28, and near-perfect accuracy (99.17%) at layer 31. This demonstrates that Whisper encodes speech versus non-speech as a fundamental, linearly separable distinction in its decoder residual stream, despite generating confident transcriptions for both input types.

These findings suggest that trained linear probes could provide real-time speech detection metadata alongside transcriptions, enabling systems to identify and flag potentially hallucinated outputs during inference. See Appendix for detailed dataset construction and full probing results.

4.3 Analyzing Acoustic, Contextual, and Semantic Mechanisms

It is well established that the Whisper decoder functions as a weak language model (Peng et al. 2023; Reid 2023), primarily responsible for generating transcriptions based on semantic context rather than purely

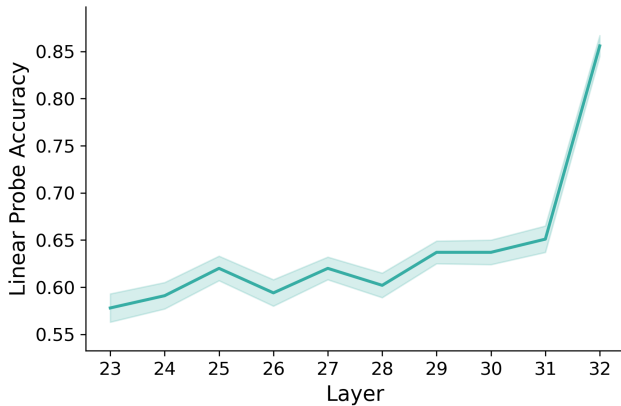


Figure 1: *Whisper encoder understands semantics*: Average linear probe accuracy (\pm SEM) across encoder layers for semantic classification.

acoustic cues (Radford et al. 2023). The encoder, in contrast, is tasked with capturing the acoustic properties of the input audio (Liu, Yang, and Qu 2024). This apparent division of roles is widely assumed in encoder–decoder ASR systems, yet the extent to which the encoder influences the final transcription output remains largely unexplored.

Acoustic and Contextual Mechanism. In the following experiment, we examine whether the model favors the acoustically spoken word, or a more contextually plausible alternative. To investigate the acoustic–contextual mechanism tradeoff, we construct a dataset of synthetic audio samples generated using a text to speech model.

Each sentence is designed to trigger contextual errors in the model, containing an acoustically ambiguous word: the true spoken word is atypical or contextually unexpected, while a more plausible word with similar phonetics fits the surrounding context. For example, a speaker may say “*white lice*” (acoustic truth) in a context where “*white rice*” would be expected. The constructed dataset consists of 700 such examples in total. The Whisper model made contextual errors on 153 examples, which we analyze to understand the underlying mechanism. Qwen2-Audio produced errors on 251 instances, indicating a stronger tendency toward contextual predictions compared to Whisper. In both cases, the model’s output differs from the ground truth by a single target word, enabling precise analysis of the acoustic–contextual tradeoff.

Next, we perform *component patching* across all encoder and decoder subcomponents on the 251 Qwen2-Audio cases and 153 Whisper cases. Motivated by established intervention methods 3.2, we select a white noise audio as the disruptive audio, \mathbf{x}^{dis} (see Section 3).

Surprisingly, applying patching interventions to encoder components using disruptive audio improves acoustic accuracy, despite the common assumption that

Metric	Whisper	Qwen2-Audio
Error Cases	153/700 (21.8%)	251/700 (35.8%)
Restored Acc.	136/153 (88.9%)	176/251 (70.1%)
Via Encoder	130/153 (85.0%)	171/251 (68.1%)
Via Decoder	126/153 (82.4%)	147/251 (58.6%)

Table 1: Acoustic–contextual patching results using white noise disruption.

encoders operate purely on acoustic input, without encoding contextual or semantic information (Table 1). Both encoder and decoder components contributed to restoring acoustic accuracy, with encoders showing particularly strong effectiveness across both models.

These findings indicate that the encoder is not limited to acoustic processing, it also encodes contextual and semantic expectations that can bias the model toward more likely completions. In fact, intervening on the encoder improves transcription accuracy in many cases, providing direct evidence that semantic influence originates in the encoder and that not all contextual decisions are made in the decoder.

Whisper Encoder Understands Semantics. Following our findings that disrupting encoder components paradoxically improves acoustic transcription, here, we aim at investigating whether ASR encoders encode semantic information. To that end, we design and construct a dedicated synthetic audio dataset. The dataset consists of carefully selected terms from distinct semantic groups, e.g., fruits and clothing. Next, we train linear probes to discriminate between pairs of these semantic categories based solely on encoder activations.

The probe results demonstrated a clear pattern: semantic encoding becomes increasingly prominent in higher encoder layers. Figure 1 shows the mean classification accuracy across 66 semantic category pairs, with many individual pairs achieving exceptional performance. Remarkably, Figure 2 reveals that semantic understanding emerges as early as the middle encoder layers (18–21), with several category pairs already achieving substantial performance well before the final layers. This early semantic emergence demonstrates a gradual build-up of semantic representations throughout the encoder hierarchy.

In the last encoder layer, probes reached their peak semantic understanding, with average accuracy of 85.6%. Several category pairs achieving 96.7% accuracy (e.g., distinguishing *countries* from *weather* or *clothing*), while maintaining strong performance across most semantic distinctions. The progression from early semantic signals to sophisticated categorical distinctions suggests that the encoder develops hierarchical semantic representations alongside its acoustic processing capabilities. Full evaluation details in the Appendix.

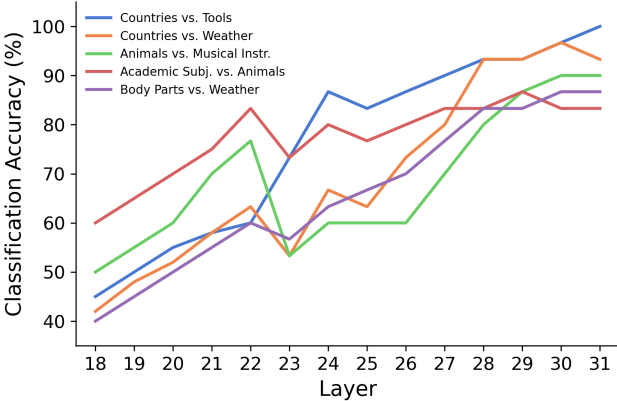


Figure 2: Semantic classification progression across encoder layers for selected category pairs.

4.4 Token Selection Mechanism

In this section, we explore the internal mechanism that underlies token selection within the decoder. Our aim is to understand when the model determines which tokens to output. To this end, we apply the *logit lens* technique to analyze model’s behavior. Specifically, we evaluate both Whisper and Qwen2-Audio in six languages: English, French, Spanish, German, Chinese and Italian. For each language, we randomly sample 100 utterances from the CommonVoice (Ardila et al. 2020) test set, resulting in a balanced multilingual evaluation set.

Token Selection Dynamics. We start by examining how the probability assigned to the final selected token changes across different layers. Figure 3a presents the mean probability averaged across examples from all the six languages and token positions. For both Whisper and Qwen2-Audio, the probability remains low until around layer 20, after which it increases sharply, with the final three layers showing high confidence in the selected token. We also analyze the saturation layer (Lioubashevski et al. 2024), defined in Section 3. Interestingly, although the mean probability of the selected token is generally higher in Qwen2-Audio, the saturation layer tends to appear earlier in Whisper. We provide additional results of the token selection by language in the Appendix.

Acoustic and Semantic Token Similarity. Both Whisper and Qwen2-Audio generate transcripts as sequences of subword tokens, in contrast to models such as (Baevski et al. 2020) that operate at the grapheme level. Given that tokens can differ in phonetic and acoustic content, we extend our analysis by comparing the acoustic distance and semantic similarity between the final selected token and the top five candidate tokens produced by the model at each layer. For acoustic distance, we use a modified version of the Phoneme Error Rate (PER) metric. As with the standard PER, lower values indicate higher acoustic similarity. For semantic similarity, we compute cosine similarity between

token embeddings. Details on how these metrics are calculated appear in the Appendix.

Figure 3b shows that across all layers, Whisper consistently achieves lower PER scores than Qwen2-Audio, suggesting higher acoustic similarity to the final selected token. Both models also display a notable PER drop around layer 25, aligning with the saturation point where predictions stabilize. This suggests that from layer 25 onward, not only does the model converge on the final prediction, but the other top-5 candidate tokens also share closer acoustic characteristics with it.

While one might expect Qwen2-Audio to outperform in semantic similarity given its large language modeling capacity, Figure 3c reveals that Whisper actually maintains higher semantic similarity scores across most layers, indicating its top candidate tokens remain more semantically aligned with the final output.

Next-Token Prediction Capabilities. Finally, we examine the model’s ability to anticipate future tokens, i.e., tokens of future timestamps, beyond the current selection in step s . We observe that Qwen2-Audio begins ranking the immediate next token ($s+1$) among its top candidates around layer 21 and retains some predictive ability for the token at position $s+2$. In contrast, Whisper shows a later but sharper improvement, with notable gains starting around layer 29. Full details are provided in the Appendix.

4.5 Decoder Repetition Mechanisms in Whisper

Repetition hallucinations, where decoder-based models produce excessively repetitive output, are a well-documented failure mode across both language and speech domains (Barański et al. 2025; Yona et al. 2025).

Whisper occasionally produces repetitive outputs (Barański et al. 2025). Based on our observations, these phenomena occur in several specific scenarios: when the input audio itself contains repetitive content (e.g., saying ‘hey’ ten times results in Whisper generating hundreds of repetitions), during code-switching between languages, and when processing fragmented, heavily noised, or completely unclear audio inputs (see examples in Appendix).

We hypothesized that such hallucinations stem from specific components within the decoder’s attention mechanisms, rather than being the result of a distributed failure across the model. To test this, we apply both causal patching and ablation interventions (See section 3.2) on the Whisper model. For each of the decoder’s 32 layers, we modified the outputs of three core components: cross-attention, self-attention, and feed-forward layers. Patching involved replacing internal activations with those from clean, non-repetitive reference audio, while ablation zeroed out the original activations. For evaluation, we construct a multilingual dataset of 102 utterances prone to repetition hallucinations, sampled from the Japanese and English portions of CommonVoice 16.1. (Ardila et al. 2020).

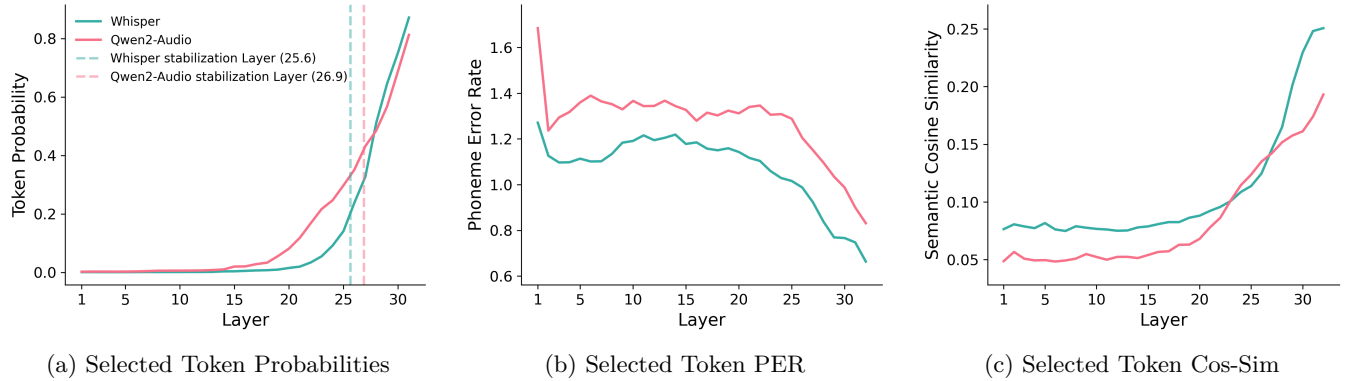


Figure 3: *Token Selection Mechanism*: (a) Probability of the final selected token across decoder layers, with indication to the average saturation layer; (b) Phoneme error rate (PER) by layer. Lower PER indicates higher acoustic similarity; (c) Tokens semantic cosine similarity by layer. Higher similarity indicates greater semantic similarity between top-5 tokens.

Our results show that intervening on cross-attention substantially reduced repetitions. Patching in layer 23 resolved 76% of cases, and layer 18 covered an additional 13%. Self-attention and fully-connected interventions had no measurable effect. Moreover, a head-level analysis revealed that head 13 in layer 18 was especially influential, suppressing repetition by 78.1% when targeted alone. This single-head effectiveness represents a remarkably focused intervention: out of 640 total attention heads in the model (32 layers \times 20 heads), one specific head in the cross-attention mechanism appears to play a disproportionately critical role in repetition control. Combined, layer 23 and head 13 in layer 18 accounted for 89% of the corrected examples.

The concentration of repetition control in specific cross-attention components reveals these hallucinations are highly localized. The remarkable effectiveness of a single attention head demonstrates significant progress toward mechanistic understanding and enables targeted interventions - these components can be monitored, steered, or fine-tuned to suppress errors without degrading core performance.

4.6 Encoder Lens

In this experiment, we aim to gain a deeper understanding of how representations evolve across the encoder layers. To this end, we use the *encoder lens* technique described in Section 3.2, which involves omitting the top layers of the encoder and directly passing intermediate representations to the decoder. We analyzed 400 audio samples for both Whisper and Qwen2-Audio, drawn from English (LibriSpeech, Panayotov et al. (2015)), Spanish (Multilingual LibriSpeech, Pratap et al. (2020)), and Chinese (AISHELL, Bu et al. (2017)). These samples were randomly selected to ensure typological and phonetic diversity across languages and datasets.

The results show that Whisper exhibits a highly structured representational hierarchy. Layers 0 to 22

mainly produce empty strings or isolated punctuations. At the later layers, the model sometimes produces short, often incomplete, words or monosyllabic tokens, that sometimes match the beginning of the actual utterance. We observe a recurring phenomenon at the 20th layer and up to the 27th: the model occasionally outputs syntactically well-formed phrases. The start of the phrases resemble to the start of the audio content, followed with unrelated text. This text, however, is grammatically correct. For example, in one of the samples, the full correct phrase is: Yes, I need repose. Many things have agitated me today, both in mind and body. When you return tomorrow, I shall no longer be the same man. and the output of the 26 layer is: Yes, I need to go to the bathroom. Which is grammatically coherent but does not match the content in the original audio. This suggests that in this mid-layer zone, Whisper may begin to behave like a loosely grounded language model, producing fluent but unanchored completions (Chen et al. 2024). Another interesting pattern we observed begins at the 27th encoder layer, where the model starts to fall into repetition loops. This phenomenon is consistent across all languages. This behavior intensifies through the 30th layer, which appears to be the most consistently affected. In our Whisper analysis, around 60% of the samples showed this repetition pattern. Only in the final layers (31st and 32nd) these repetitions resolve into fluent, grammatically correct transcriptions.

Qwen2-Audio, in contrast, reveals different failure patterns. While the last five layers reliably generate accurate transcriptions, earlier layers show severe degradation. We perform a frequency analysis of the Qwen2-Audio results, which reveals a surprising phenomenon: the phrase Kids are talking by the door (potentially from the RAVDESS (Livingstone and Russo 2018) dataset for emotion detection) appears at least once in 390 out of 400 files, regardless of the input lan-

guage. This phenomenon is signaling a strongly memorized training data in the model. Alongside it, several high-frequency Chinese expressions which roughly translates to Aren't you bored being alone?) dominate the output in the earlier layers. We provide additional examples in the Appendix.

These patterns suggest that the model reverts to memorized sequences when uncertain, possibly due to training data imbalance.

5 Discussion

This work provides a first comprehensive exploration of interpretability in modern ASR models. We show that a range of acoustic, semantic, and contextual factors are internally represented and can be analyzed using adapted techniques from LLM interpretability. Our experiments uncover localized mechanisms behind hallucinations, repetition loops, and context-driven errors, and offer new tools for inspecting how predictions evolve across layers.

We demonstrate the potential of interpretability for advancing diverse future research in ASR. These include building internal monitors for hallucination or saturation, developing fine-grained editing and debugging tools for ASR, and informing architectural choices that better balance grounding and fluency. The ability to trace errors back to individual components may also enable targeted interventions or model compression strategies.

References

Abouelenin, A.; Ashfaq, A.; Atkinson, A.; Awadalla, H.; Bach, N.; Bao, J.; Benhaim, A.; Cai, M.; Chaudhary, V.; Chen, C.; et al. 2025. Phi-4-mini technical report: Compact yet powerful multimodal language models via mixture-of-loras. *arXiv preprint arXiv:2503.01743*.

Ardila, R.; Branson, M.; Davis, K.; Henretty, M.; Kohler, M.; Meyer, J.; Morais, R.; Saunders, L.; Tyers, F. M.; and Weber, G. 2020. Common Voice: A Massively-Multilingual Speech Corpus. *arXiv:1912.06670*.

Baevski, A.; Zhou, Y.; Mohamed, A.; and Auli, M. 2020. wav2vec 2.0: A framework for self-supervised learning of speech representations. *Advances in neural information processing systems*, 33: 12449–12460.

Ballier, N.; Burin, L.; Namdarzadeh, B.; Ng, S.; Wright, R.; and Yunès, J.-B. 2024. Probing Whisper predictions for French, English and Persian transcriptions. In *7th International Conference on Natural Language and Speech Processing*, 129–138. Association for Computational Linguistics.

Barański, M.; Jasiński, J.; Bartolewska, J.; Kacprzak, S.; Witkowski, M.; and Kowalczyk, K. 2025. Investigation of whisper asr hallucinations induced by non-speech audio. In *ICASSP 2025-2025 IEEE International Conference on Acoustics, Speech and Signal Processing (ICASSP)*, 1–5. IEEE.

Barbero, F.; Banino, A.; Kapturowski, S.; Kumaran, D.; Madeira Araújo, J.; Vitvitskyi, O.; Pascanu, R.; and Veličković, P. 2024. Transformers need glasses! information over-squashing in language tasks. *Advances in Neural Information Processing Systems*, 37: 98111–98142.

Belinkov, Y. 2022. Probing classifiers: Promises, shortcomings, and advances. *Computational Linguistics*, 48(1): 207–219.

Belrose, N.; Furman, Z.; Smith, L.; Halawi, D.; Ostrovsky, I.; McKinney, L.; Biderman, S.; and Steinhardt, J. 2023. Eliciting latent predictions from transformers with the tuned lens. *arXiv preprint arXiv:2303.08112*.

Ben Melech Stan, G.; Aflalo, E.; Rohekar, R. Y.; Bhawandiwala, A.; Tseng, S.-Y.; Olson, M. L.; Gurwicz, Y.; Wu, C.; Duan, N.; and Lal, V. 2024. Lvlm-intrep: An interpretability tool for large vision-language models. In *Proceedings of the IEEE/CVF Conference on Computer Vision and Pattern Recognition*, 8182–8187.

Bernard, M.; and Titeux, H. 2021. Phonemizer: Text to Phones Transcription for Multiple Languages in Python. *Journal of Open Source Software*, 6(68): 3958.

Berns, T.; Vaessen, N.; and van Leeuwen, D. A. 2023. Speaker and language change detection using wav2vec2 and whisper. *arXiv preprint arXiv:2302.09381*.

Bojanowski, P.; Grave, E.; Joulin, A.; and Mikolov, T. 2017. Enriching Word Vectors with Subword Information. *Transactions of the Association for Computational Linguistics*, 5: 135–146.

Brown, T.; Mann, B.; Ryder, N.; Subbiah, M.; Kaplan, J. D.; Dhariwal, P.; Neelakantan, A.; Shyam, P.; Sastry, G.; Askell, A.; et al. 2020. Language models are few-shot learners. *Advances in neural information processing systems*, 33: 1877–1901.

Bu, H.; Du, J.; Na, X.; Wu, B.; and Zheng, H. 2017. Aishell-1: An open-source mandarin speech corpus and a speech recognition baseline. In *2017 20th conference of the oriental chapter of the international coordinating committee on speech databases and speech I/O systems and assessment (O-COCOSDA)*, 1–5. IEEE.

Chen, A.; Zhang, R.; Pan, J.; Yu, F. F.; He, Y.; Wang, Y.; Neubig, G.; and Lee, J. D. 2024. Language Emerges in Speech Models Trained Without Text Supervision. *arXiv preprint arXiv:2503.08908*.

Chu, Y.; Xu, J.; Yang, Q.; Wei, H.; Wei, X.; Guo, Z.; Leng, Y.; Lv, Y.; He, J.; Lin, J.; et al. 2024. Qwen2-audio technical report. *arXiv preprint arXiv:2407.10759*.

Chu, Y.; Xu, J.; Zhou, X.; Yang, Q.; Zhang, S.; Yan, Z.; Zhou, C.; and Zhou, J. 2023. Qwen-Audio: Advancing Universal Audio Understanding via Unified Large-Scale Audio-Language Models. *arXiv preprint arXiv:2311.07919*.

Das, N.; Dingliwal, S.; Ronanki, S.; Paturi, R.; Huang, Z.; Mathur, P.; Yuan, J.; Bekal, D.; Niu, X.; Jayanthi, S. M.; et al. 2024. Speechverse: A large-scale

generalizable audio language model. *arXiv preprint arXiv:2405.08295*.

Fonseca, E.; Favery, X.; Pons, J.; Font, F.; and Serra, X. 2021. Fsd50k: an open dataset of human-labeled sound events. *IEEE/ACM Transactions on Audio, Speech, and Language Processing*, 30: 829–852.

Frieske, R.; and Shi, B. E. 2024. Hallucinations in neural automatic speech recognition: Identifying errors and hallucinatory models. *arXiv preprint arXiv:2401.01572*.

Geva, M.; Caciularu, A.; Wang, K. R.; and Goldberg, Y. 2022. Transformer feed-forward layers build predictions by promoting concepts in the vocabulary space. *arXiv preprint arXiv:2203.14680*.

Goldowsky-Dill, N.; MacLeod, C.; Sato, L.; and Arora, A. 2023. Localizing model behavior with path patching. *arXiv preprint arXiv:2304.05969*.

Gong, Y.; Khurana, S.; Karlinsky, L.; and Glass, J. 2023. Whisper-at: Noise-robust automatic speech recognizers are also strong general audio event taggers. *arXiv preprint arXiv:2307.03183*.

Haklay, T.; Orgad, H.; Bau, D.; Mueller, A.; and Belinkov, Y. 2025. Position-aware automatic circuit discovery. *arXiv preprint arXiv:2502.04577*.

Hanna, M.; Liu, O.; and Variengien, A. 2023. How does GPT-2 compute greater-than?: Interpreting mathematical abilities in a pre-trained language model. *Advances in Neural Information Processing Systems*, 36: 76033–76060.

Heimersheim, S.; and Nanda, N. 2024. How to use and interpret activation patching. *arXiv preprint arXiv:2404.15255*.

Hernandez, E.; Sharma, A. S.; Haklay, T.; Meng, K.; Wattenberg, M.; Andreas, J.; Belinkov, Y.; and Bau, D. 2023. Linearity of relation decoding in transformer language models. *arXiv preprint arXiv:2308.09124*.

Kim, C. D.; Kim, B.; Lee, H.; and Kim, G. 2019. Audio-caps: Generating captions for audios in the wild. In *Proceedings of the 2019 Conference of the North American Chapter of the Association for Computational Linguistics: Human Language Technologies, Volume 1 (Long and Short Papers)*, 119–132.

Kramár, J.; Lieberum, T.; Shah, R.; and Nanda, N. 2024. Atp*: An efficient and scalable method for localizing llm behaviour to components. *arXiv preprint arXiv:2403.00745*.

Lioubashevski, D.; Schlank, T.; Stanovsky, G.; and Goldstein, A. 2024. Looking beyond the top-1: Transformers determine top tokens in order. *arXiv preprint arXiv:2410.20210*.

Liu, Y.; Yang, X.; and Qu, D. 2024. Exploration of Whisper fine-tuning strategies for low-resource ASR. *EURASIP Journal on Audio, Speech, and Music Processing*, 2024(1): 29.

Livingstone, S. R.; and Russo, F. A. 2018. The Ryerson Audio-Visual Database of Emotional Speech and Song (RAVDESS): A dynamic, multimodal set of facial and vocal expressions in North American English. *PloS one*, 13(5): e0196391.

Luo, H.; and Specia, L. 2024. From Understanding to Utilization: A Survey on Explainability for Large Language Models. *ArXiv*, abs/2401.12874.

McKenzie, A.; Pawar, U.; Blandfort, P.; Banks, W.; Krueger, D.; Lubana, E. S.; and Krasheninnikov, D. 2025. Detecting High-Stakes Interactions with Activation Probes. *arXiv preprint arXiv:2506.10805*.

Meng, K.; Bau, D.; Andonian, A.; and Belinkov, Y. 2022. Locating and editing factual associations in gpt. *Advances in neural information processing systems*, 35: 17359–17372.

Nanda, N. 2023. Attribution patching: Activation patching at industrial scale. *URL: https://www.neelnanda.io/mechanistic-interpretability/attribution-patching*.

nostalgiaist. 2020. Interpreting GPT: the logit lens. <https://www.lesswrong.com/posts/AcKRB8wDpdAN6v6ru/interpreting-gpt-the-logit-lens>. Accessed: 2025-07-30.

O’Neill, C.; Chalnev, S.; Zhao, C. C.; Kirkby, M.; and Jayasekara, M. 2025. A Single Direction of Truth: An Observer Model’s Linear Residual Probe Exposes and Steers Contextual Hallucinations. *arXiv:2507.23221*.

Orgad, H.; Toker, M.; Gekhman, Z.; Reichart, R.; Szpektor, I.; Kotek, H.; and Belinkov, Y. 2024. Llms know more than they show: On the intrinsic representation of llm hallucinations. *arXiv preprint arXiv:2410.02707*.

Panayotov, V.; Chen, G.; Povey, D.; and Khudanpur, S. 2015. Librispeech: An ASR corpus based on public domain audio books. In *2015 IEEE International Conference on Acoustics, Speech and Signal Processing (ICASSP)*, 5206–5210.

Peng, Y.; Tian, J.; Yan, B.; Berrebbi, D.; Chang, X.; Li, X.; Shi, J.; Arora, S.; Chen, W.; Sharma, R.; et al. 2023. Reproducing whisper-style training using an open-source toolkit and publicly available data. In *2023 IEEE Automatic Speech Recognition and Understanding Workshop (ASRU)*, 1–8. IEEE.

Pratap, V.; Xu, Q.; Sriram, A.; Synnaeve, G.; and Collobert, R. 2020. MLS: A Large-Scale Multilingual Dataset for Speech Research. In *Interspeech 2020*. ISCA.

Radford, A.; Kim, J. W.; Xu, T.; Brockman, G.; McLeavey, C.; and Sutskever, I. 2023. Robust speech recognition via large-scale weak supervision. In *International conference on machine learning*, 28492–28518. PMLR.

Räuker, T.; Ho, A.; Casper, S.; and Hadfield-Menell, D. 2023. Toward transparent ai: A survey on interpreting the inner structures of deep neural networks. In *2023 ieee conference on secure and trustworthy machine learning (satml)*, 464–483. IEEE.

Reid, E. 2023. Interpreting OpenAI’s Whisper. <https://www.lesswrong.com/posts/thePw6qdyabD8XR4y/interpreting-openai-s-whisper>. LessWrong / SERIMATS blog post.

Schut, L.; Gal, Y.; and Farquhar, S. 2025. Do Multilingual LLMs Think In English? *arXiv preprint arXiv:2502.15603*.

Snyder, D.; Chen, G.; and Povey, D. 2015. Musan: A music, speech, and noise corpus. *arXiv preprint arXiv:1510.08484*.

Syed, A.; Rager, C.; and Conmy, A. 2023. Attribution patching outperforms automated circuit discovery. *arXiv preprint arXiv:2310.10348*.

Tang, C.; Yu, W.; Sun, G.; Chen, X.; Tan, T.; Li, W.; Lu, L.; Ma, Z.; and Zhang, C. 2023. Salmonn: Towards generic hearing abilities for large language models. *arXiv preprint arXiv:2310.13289*.

Team, Q. 2024. Qwen2 technical report. *arXiv preprint arXiv:2407.10671*.

Toker, M.; Orgad, H.; Ventura, M.; Arad, D.; and Belinkov, Y. 2024. Diffusion Lens: Interpreting Text Encoders in Text-to-Image Pipelines. *arXiv preprint arXiv:2403.05846*.

Touvron, H.; Lavril, T.; Izacard, G.; Martinet, X.; Lachaux, M.-A.; Lacroix, T.; Rozière, B.; Goyal, N.; Hambro, E.; Azhar, F.; et al. 2023. Llama: Open and efficient foundation language models. *arXiv preprint arXiv:2302.13971*.

Upadhyay, S. G.; Busso, C.; and Lee, C.-C. 2024. A layer-anchoring strategy for enhancing cross-lingual speech emotion recognition. *arXiv preprint arXiv:2407.04966*.

Vaswani, A.; Shazeer, N.; Parmar, N.; Uszkoreit, J.; Jones, L.; Gomez, A. N.; Kaiser, Ł.; and Polosukhin, I. 2017. Attention is all you need. *Advances in neural information processing systems*, 30.

Vig, J.; Gehrmann, S.; Belinkov, Y.; Qian, S.; Nevo, D.; Singer, Y.; and Shieber, S. 2020. Investigating gender bias in language models using causal mediation analysis. *Advances in neural information processing systems*, 33: 12388–12401.

Wang, H. ???? English Accent DataSet. https://huggingface.co/datasets/westbrook/English_Accent_DataSet. Accessed: 2025-07-31.

Wang, K.; Variengien, A.; Conmy, A.; Shlegeris, B.; and Steinhardt, J. 2022. Interpretability in the wild: a circuit for indirect object identification in gpt-2 small. *arXiv preprint arXiv:2211.00593*.

Yang, C.-K.; Huang, K.-P.; and Lee, H.-y. 2024. Do Prompts Really Prompt? Exploring the Prompt Understanding Capability of Whisper. *arXiv preprint arXiv:2406.05806*.

Yona, I.; Shumailov, I.; Hayes, J.; Barbero, F.; and Gandlerman, Y. 2025. Interpreting the Repeated Token Phenomenon in Large Language Models. *arXiv preprint arXiv:2503.08908*.

Zhao, Y.; Wang, S.; Sun, G.; Chen, Z.; Zhang, C.; Xu, M.; and Zheng, T. F. 2024. Whisper-pmfa: Partial multi-scale feature aggregation for speaker verification using whisper models. *arXiv preprint arXiv:2408.15585*.

Appendix: Beyond Transcription—Mechanistic Interpretability in ASR

A Detailed Probing Results

This section presents comprehensive layer-wise analysis of various probing tasks across Whisper’s encoder and decoder layers, demonstrating the model’s ability to linearly separate different types of information at different depths.

A.1 Gender classification

Gender classification performance across encoder layers is shown in Figure 4. The results demonstrate a clear progression from random performance at the embedding layer (Layer 0: 55.5%) to peak performance at Layer 25 (94.6%), indicating that gender information becomes increasingly linearly separable in deeper encoder layers.

A.2 Clean vs. noisy environment classification

Clean vs. noisy environment classification across encoder layers is presented in Figure 5. The model shows steady improvement from Layer 0 (58.4%) reaching optimal performance at Layer 27 (90.0%), suggesting that acoustic quality indicators are most effectively captured in the deeper encoder representations.

A.3 Accent classification environment classification

Detailed accent classification results across encoder layers are provided in Table 2. The analysis covers four accent categories (New Zealand, Welsh, South African, and Indian) with peak overall accuracy achieved at Layer 22.

A.4 Speech vs. Non-Speech Classification

Speech vs. non-speech classification performance across decoder layers is illustrated in Figure 6. The results reveal remarkable performance, with perfect classification (100%) consistently achieved across Layers 10–28, and near-perfect accuracy (99.17%) maintained at Layer 31. This demonstrates the decoder’s robust ability to distinguish between genuine speech content and non-speech audio inputs.

A.5 Hallucination Prediction from Decoder Residual Stream

Word Error Rate (WER) classification results for detecting transcription quality are detailed in Table 3. The decoder residual stream analysis shows peak performance at Layer 22 (93.3% accuracy), indicating that hallucination-related signals are effectively encoded in the deeper decoder layers during generation.

B Token Selection Mechanism

Selected Token Dynamic. Figure 7 shows the mean probability of the final selected token across layers, broken down by language. The Whisper model displays

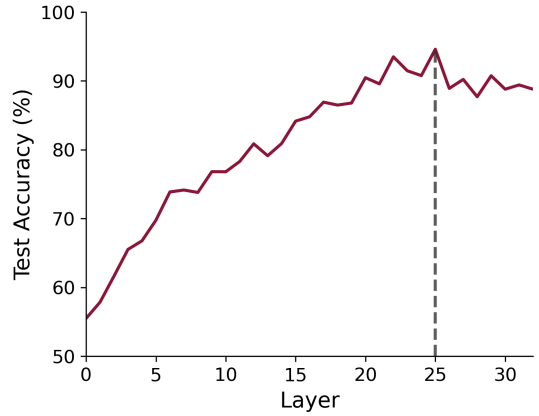


Figure 4: Gender classification test accuracy across Whisper encoder layers. Peak performance of 94.6% achieved at layer 25.

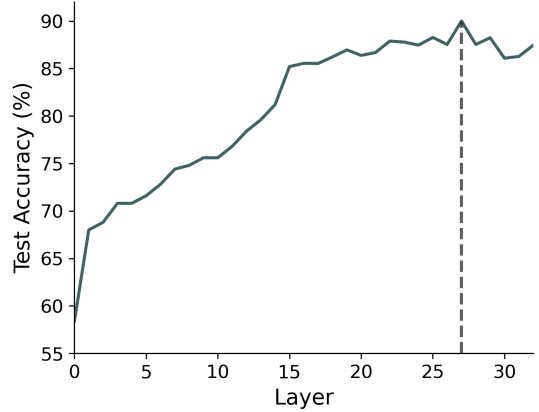


Figure 5: Clean vs noisy speech classification accuracy across Whisper encoder layers. Peak performance of 90.0% achieved at layer 27.

similar trends across all six languages, with slightly higher confidence for English and the lowest confidence for Chinese. In contrast, Qwen2-Audio exhibits a different pattern: for English and Chinese, it shows much higher confidence in earlier layers compared to the other languages.

Top-K Tokens Dynamic. Figure 8 presents how the probabilities of the top-5 tokens evolve across layers. Here, position 1 corresponds to the token with the highest probability at that layer, position 2 to the next highest, and so on.

In layer 1, Whisper is highly confident: the most probable token receives a probability of 1. However, this confidence rapidly declines, and the probabilities across all positions quickly approach zero. Around layer 22, as shown earlier, the probability of the top-ranked token

Table 2: Accent Classification by Encoder Layer

Layer	Overall	NZ	Welsh	SA	Indian
5	59.5%	38.0%	70.0%	70.0%	60.0%
10	63.0%	48.0%	70.0%	66.0%	68.0%
15	64.5%	56.0%	76.0%	66.0%	60.0%
20	79.0%	74.0%	94.0%	74.0%	74.0%
25	82.5%	84.0%	98.0%	68.0%	80.0%
28	80.5%	88.0%	96.0%	60.0%	78.0%
31	78.5%	82.0%	96.0%	64.0%	72.0%

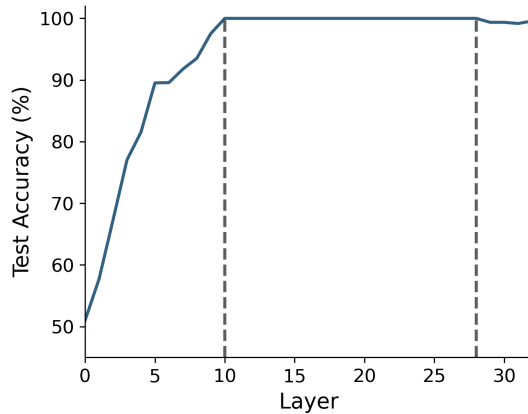
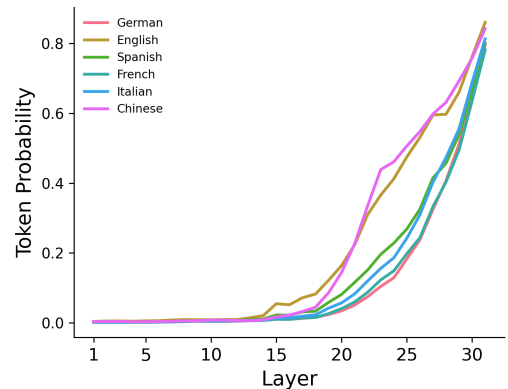


Figure 6: Speech vs non-speech classification accuracy across Whisper decoder layers. Perfect classification (100%) achieved in layers 10-28.

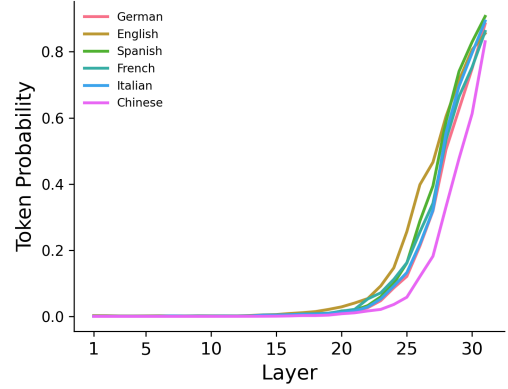
begins to rise again, eventually reaching an average of about 0.8, while the probabilities for positions 2-5 remain very low, staying close to zero.

In contrast, Qwen2-Audio exhibits a different pattern. Throughout most layers, the top-ranked token receives the highest probability, but only around 0.2. From approximately layer 20 onward, this probability starts to increase, also stabilizing around 0.8 in the final layers. Unlike Whisper, however, the token in position 2 in Qwen2-Audio maintains a probability of about 0.1 from around layer 20 onward.

Phoneme Error Rate (PER). We propose PER as an alternative to Word Error Rate (WER), computed at the phoneme level. Instead of applying a uniform penalty, substitutions between phonemes from the same family (e.g., vowels or nasals) receive a reduced penalty of 0.5 to better reflect phonetic closeness. Each token is first converted to its phoneme sequence, and tokens without acoustic content (such as punctuation or language tags) are excluded from the calculation for both Whisper and Qwen2-Audio. Deriving phonemes first requires detecting the language of each token, which is challenging given the short length of tokens. We apply a set of simple rules: tokens containing characters from the CJK Unified Ideographs range are labeled as Chinese (even though this range also includes Japanese



(a) Qwen2-Audio



(b) Whisper

Figure 7: Probability of the final selected token across decoder layers and languages for (a) Qwen2-Audio and (b) Whisper.

kanji and Korean hanja, we apply this rule because our data only include Chinese audio); tokens containing Cyrillic characters are labeled as Russian; and all other tokens are classified using fastText’s language detection (Bojanowski et al. 2017). Finally, we use Phonemizer (Bernard and Titeux 2021) to generate the corresponding phoneme sequences for each token based on its detected language. Figure 9 shows the acoustic distance, measured by phoneme error rate (PER), between the final selected token and the top five candidate tokens produced by the models at each layer, broken down by language. For both models, PER starts very high at the first layer, then remains relatively stable until around layer 21, after which it drops sharply. Overall, Whisper achieves lower PER across all languages, and both models perform best (i.e., show lower PER) on English and Chinese.

Semantic similarity. We compute semantic embeddings for each token using fastText (Bojanowski et al. 2017) and measure their cosine similarity to the final selected token. The embedding model is selected according to the language of the audio. We exclude lan-

Table 3: Hallucination Prediction from Decoder Residual Stream

Layer	Test Acc	Train Acc	Train Time (s)	Low WER F1	High WER F1
5	0.622	0.571	0.92	0.393	0.726
10	0.900	0.838	0.76	0.907	0.892
15	0.889	1.000	0.70	0.886	0.891
20	0.878	1.000	0.66	0.874	0.882
22	0.933	1.000	0.66	0.933	0.933
25	0.900	0.995	0.64	0.899	0.901
28	0.922	1.000	0.59	0.923	0.921
31	0.932	1.000	0.57	0.935	0.932

guage tokens and other special tokens (i.e., tokens in the $<|value|>$ format), but retain punctuation tokens since they can carry semantic meaning. Figure 10 shows the average cosine similarity between the final selected token and the top five candidates across layers and languages. The Whisper model displays an interesting pattern: English starts with relatively low similarity in earlier layers but reaches the highest similarity in later layers, while Chinese consistently shows the lowest similarity. In contrast, Qwen2-Audio shows higher similarity for Chinese already in earlier layers and again in the final layers, where English and Chinese lead. Notably, semantic similarity scores in Qwen2-Audio are overall lower than in Whisper. The stronger performance on Chinese in Qwen2-Audio may reflect its training on large amounts of Chinese data, whereas Whisper’s weaker results for Chinese could indicate less training data in that language.

Next-Token Prediction Capabilities To better understand the capacity of the ASR model, we evaluate its ability to predict multiple positions beyond the next immediate token at position s . We consider tokens at positions $s + i$ for all $1 \leq i \leq 5$. For each offset i , we measure how often the ground-truth token at position $s + i$ appears among the model’s top 10 predicted tokens at the corresponding layer. We use a metric we call Recall@10 to quantify the fraction of instances in which the correct future token is included within the top-ranked predictions. Figure 11 presents the results for both Whisper and Qwen2-Audio. As shown, Qwen2-Audio achieves a relatively high Recall @ 10 for $s+1$ (the immediate next token) starting from approximately layer 21, indicating that these deeper layers already encode useful information about the upcoming token. Furthermore, even for $s+2$, Qwen2-Audio maintains some predictive capability from the same layer onward, suggesting that it can anticipate tokens slightly further in the sequence. In contrast, Whisper exhibits a markedly different pattern. For $s+1$, the model shows a notable rise in Recall@10 only starting around layer 29, although this increase is steeper than that observed in the Qwen2-Audio model. Similar to Qwen2-Audio, Whisper also demonstrates some prediction capability for $s+2$.

Figure 12 presents the next-token prediction capabilities of Whisper and Qwen2-Audio on Japanese. Unlike other languages, Whisper shows an alternating pattern for Japanese: at even offsets i , the model achieves higher Recall@10 scores starting from around layer 27; whereas at odd offsets i , its prediction capability is generally weaker in deeper layers but unexpectedly higher at layer 1. This is a particularly interesting behavior, as it does not appear in the Qwen2-Audio model.

C Whisper’s Encoder Understands Semantic

This appendix provides detailed results from our linear probe experiments across 47 semantic category pairs on Whisper Large V3 encoder layers 22-31.

C.1 Experimental Setup

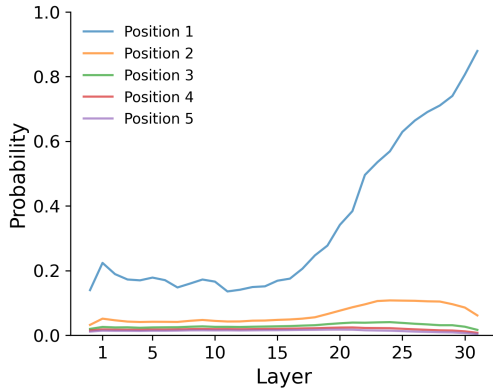
Our synthetic audio dataset comprises terms from 11 semantic categories: Animals, Tools, Fruits, Professions, Clothing, Countries, Musical Instruments, Body Parts, Weather, Transportation, and Academic Subjects. Each category contains 50 terms synthesized with consistent voice parameters. We train binary linear classifiers on 768-dimensional encoder representations using L2 regularization ($\lambda = 0.01$) and evaluate on held-out test sets.

Category Pair	Accuracy
Countries vs. Tools	100.0%
Countries vs. Clothing	100.0%
Musical Instr. vs. Countries	96.7%
Countries vs. Weather	93.3%

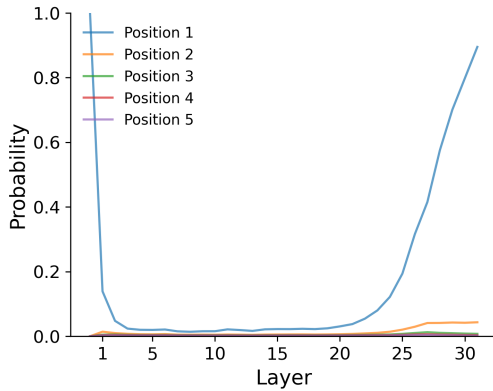
Table 4: Top Performing Category Pairs (Layer 31)

C.2 Visual Analysis

Figure 2 illustrates semantic classification progression for selected high-performing category pairs. Tables 4 and 5 summarize these results, showing perfect separation for several category pairs and consistently higher averages for *Countries* compared to other categories.



(a) Qwen2-Audio



(b) Whisper

Figure 8: Probability of the top 5 tokens across layers for (a) Qwen2-Audio and (b) Whisper.

Category	Average Accuracy
Countries	91.2%
Professions	84.2%
Body Parts	82.7%
Academic Subjects	73.0%
Clothing	72.6%

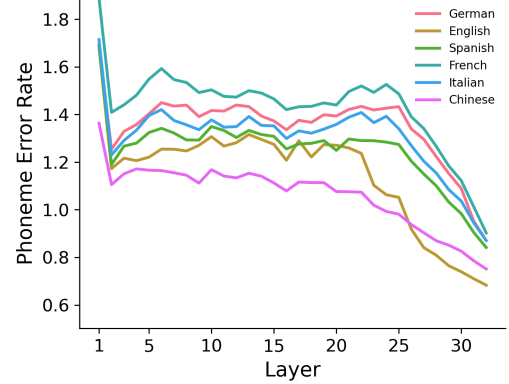
Table 5: Average Category Performance (Layer 31)

D Repetitions

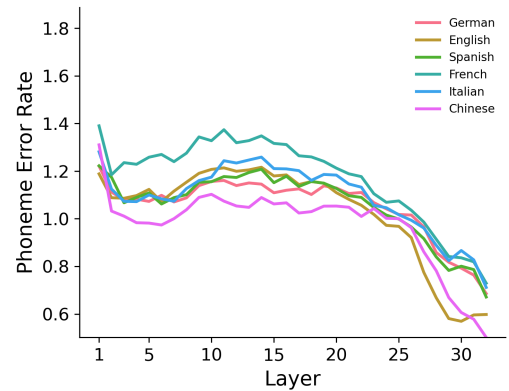
D.1 Layer 18 Norm Patterns During Repetition

Our analysis reveals distinctive activation patterns in Layer 18 during repetitive sequences that provide insights into the underlying mechanisms of repetition generation. Figure 13 shows L2 norm traces for cross-attention and self-attention components across layers 17, 18, and 19 during a repetitive sequence.

Cross-Attention as Repetition Trigger Layer 18's cross-attention component shows intense initial activation followed by sustained decline (Figure 13, top



(a) Qwen2-Audio



(b) Whisper

Figure 9: Phoneme Error Rate by layer and language for (a) Qwen2-Audio and (b) Whisper.

panel). This pattern suggests that cross-attention initially attempts to maintain alignment with the audio source but progressively loses this connection as repetition begins.

The declining cross-attention norms indicate a triggering mechanism where the encoder-decoder alignment breaks down, initiating the repetitive state.

Self-Attention as Repetition Manifestation The simultaneous elevation in self-attention norms that persists throughout repetition (Figure 13, bottom panel) reflects the decoder's internal repetitive processing.

This sustained activity pattern manifests the pathological state where the decoder becomes internally focused on repetitive patterns rather than attending to new audio input. The persistent elevation suggests that self-attention captures and maintains the repetitive behavior once initiated.

Intervention Implications The effectiveness of cross-attention patching versus self-attention intervention failure can be understood through this dual-component view.

We hypothesize that cross-attention interventions

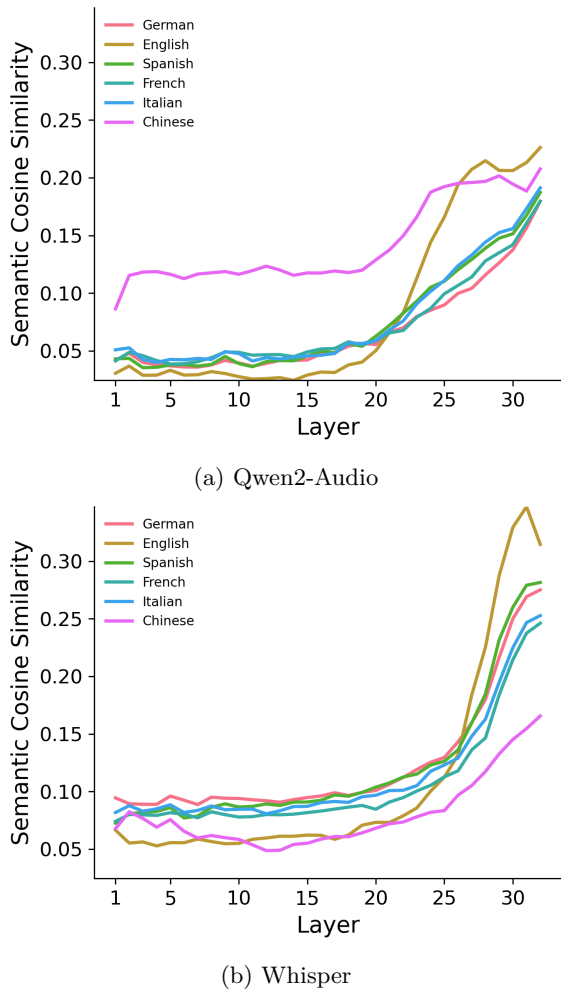


Figure 10: Tokens semantic cosine similarity by layer and language for (a) Qwen2-Audio and (b) Whisper.

target the trigger mechanism, preventing the initial breakdown in audio alignment. In contrast, self-attention interventions attempt to modify the manifestation after the repetitive state has already been established, proving less effective. Layer 18's distinctive signature in both components (Figure 13) explains why interventions at this specific layer are most effective for repetition control.

Further investigation into this trigger-manifestation mechanism could provide deeper insights into the architectural foundations of hallucination control in ASR models.

D.2 Types Of Repetitions

- Code Switching:

- **Repetitive Audio:** In the acoustic the word "ha" was said 5 times:

- **Short Noise:**

E Encoder Lens

We provide qualitative examples of decoder outputs from different encoder layers using the Whisper or Qwen2-Audio models, across three languages: Spanish, English, and Chinese, shown in Figures 15, 16 and 17 respectively.

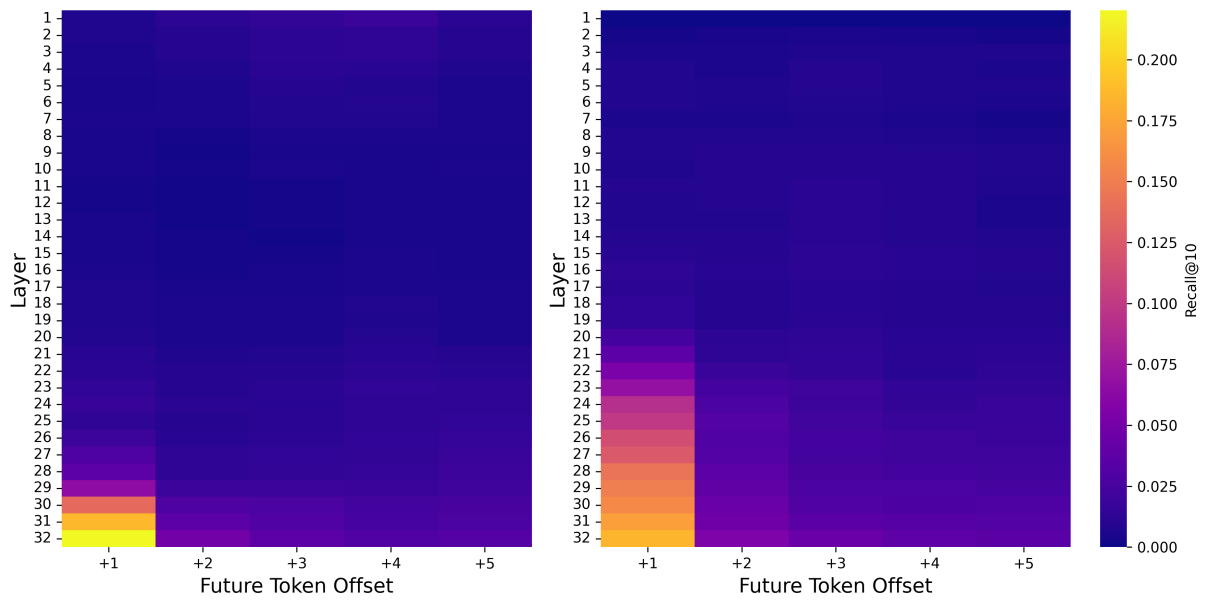


Figure 11: Future token prediction heatmap showing Recall@10 across layers i and offsets i for Whisper (left) and Qwen2-Audio (right)

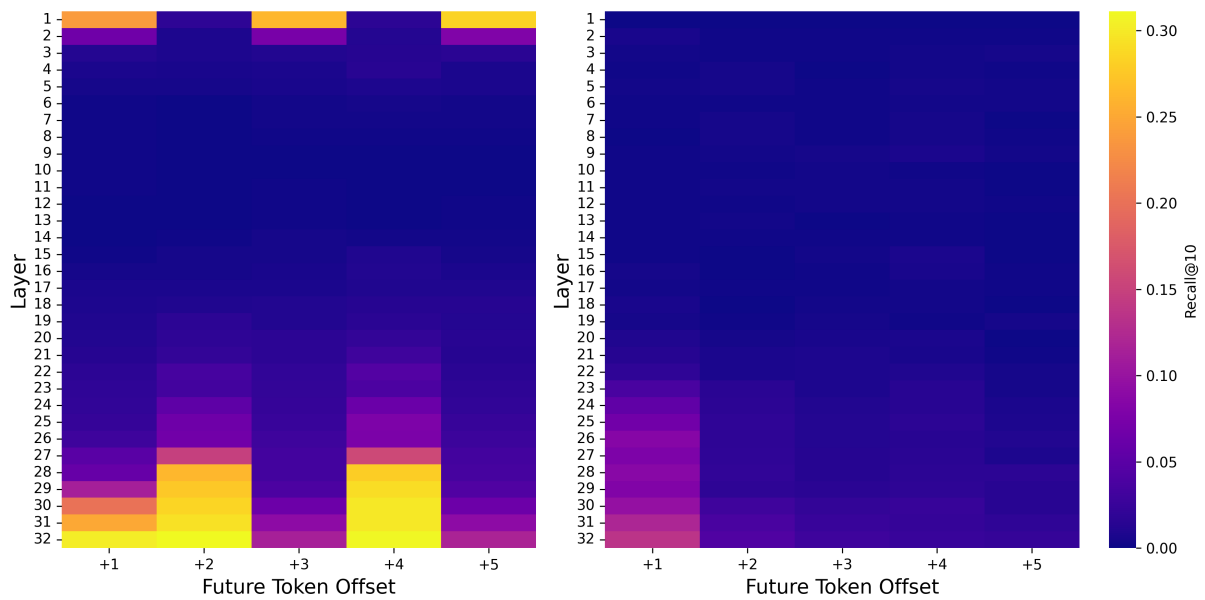


Figure 12: Japanese future token prediction heatmap showing Recall@10 across layers i and offsets i for Whisper (left) and Qwen2-Audio (right)

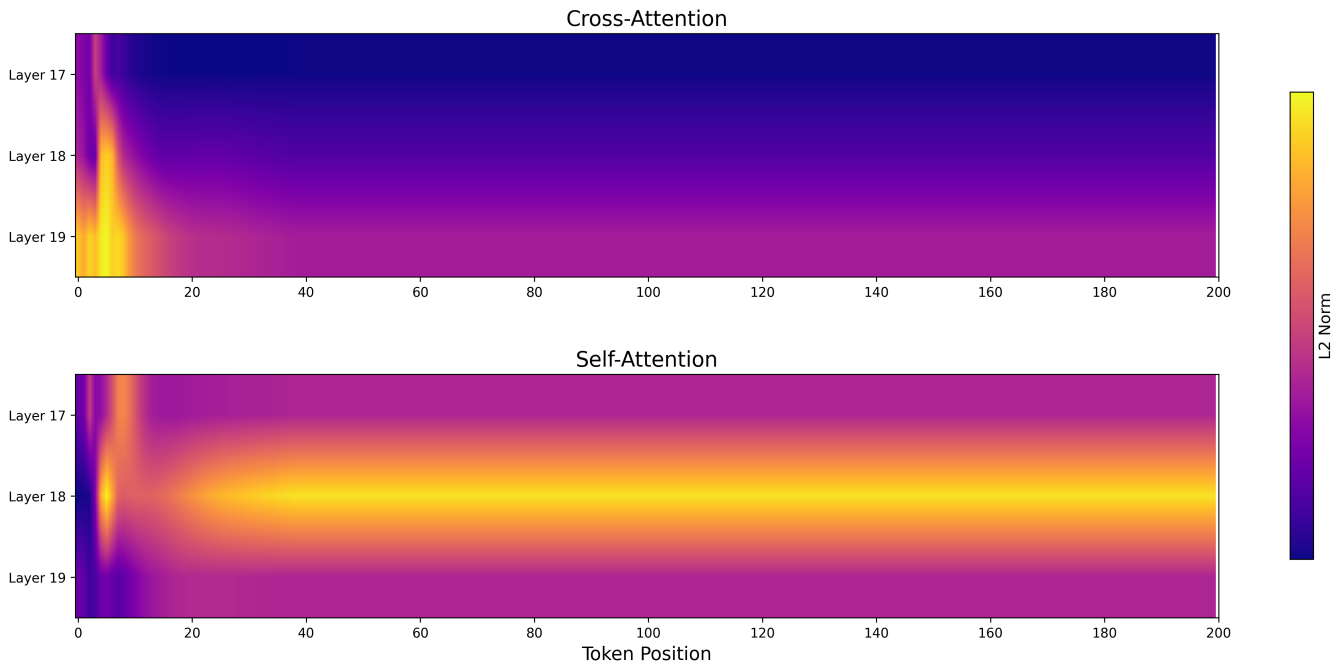


Figure 13: Attention component L2 norm traces during repetitive sequence generation. Cross-attention (top) shows peak-then-decline pattern while self-attention (bottom) exhibits sustained elevation, with Layer 18 demonstrating the most pronounced dual signature.

Default Phrase	Translation	Total	English	Spanish	Chinese	Language
Kids are talking by the door	(English)	390	83	44	263	All languages
你一个人不是很无聊吗	Aren't you bored being alone?	396	83	44	203	All languages
我告诉你那个不是真的	I tell you that's not real	309	33	23	147	All languages
我没事的表情	My it's-nothing expression	177	32	24	121	All languages
比盟啊	(Unclear Chinese phrase)	219	89	95	35	All languages
他不喝酒精类饮料	He doesn't drink alcoholic beverages	127	16	3	108	All languages
一九四九年十月一日	October 1st, 1949	121	3	3	115	Primarily Chinese
想找个女对手	Want to find a female opponent	113	81	1	31	Primarily English & Chinese
你家水稻儿栽完啦	Have you finished planting rice?	65	5	1	59	Primarily Chinese
有病啊你	Are you sick? (colloquial)	24	10	0	14	English & Chinese only

Figure 14: Examples of Frequent Default Phrases in Qwen2-Audio

Layer	Content
32	Todo el día de hoy he sido atormentada por los más horribles pensamientos de muerte y de sudarios cubiertos de sangre, hasta producirme fiebre y delirio. Por la noche he querido distraerme leyendo hasta llegar la hora, y he visto las mismas cosas en el libro.
31	Todo el día de hoy he sido atormentada por los más horribles pensamientos de muerte y de sudarios cubiertos de sangre, hasta producirme fiebre y delirio. Por la noche he querido distraerme leyendo hasta llegar la hora, y he visto las mismas cosas en el libro.
30	todo el día de hoy he sido atormentada por los más horribles pensamientos de muerte y de sufrimiento, hasta producirme fiebre y delirio. por la noche he querido distraerme leyendo hasta llegar la hora, y he visto las mismas cosas en el libro.
29	toda el día de hoy es sido atormentado por los más horribles pensamientos de muerte y de sufrimiento, y de destrucción.
28	toda la day i'm sad and lonely for the most part.
27	todd elmore is a director of photography who has worked on many notable films.
26	The person says '我告诉你那个不是真的' in Mandarin.
25	tudor eliot
24	The person says '我告诉你那个不是真的' in Mandarin.
23	The person says 'Kids are talking by the door'.
22	The person says 'Kids are talking by the door'.
21	The person says 'Kids are talking by the door'.
20	The person says 'Kids are talking by the door'.
19	Kids are talking by the door
18	沉香
17	Kids are talking by the door
16	Machiko Ono
15	Kids are talking by the door
14	The person says 'Kids are talking by the door' in English.
13	吃烧烤时应该注意什么?
12	比盟啊
11	what's up everybody i'm back with another video and today we're going to be building a very simple game using the unity engine so if you're new to unity or just want to learn how to build a simple game in a short amount of time then this video is perfect for you...
10	The transcription of the speech is '比盟啊'.
9	The transcription of the speech is '对呀'.
8	The person says 'Kids are talking by the door'.
7	The person says 'Kids are talking by the door'.
6	The person says 'Kids are talking by the door'.
5	你一个人不是很无聊吗
4	The person says '你一个人不是很无聊吗'.
3	The person says, 'Kids are talking by the door'.
2	The person says, 'Kids are talking by the door'.
1	The person says 'Kids are talking by the door'.
0	The person says, 'Kids are talking by the door'.

Figure 15: Spanish Example - Qwen2-Audio

Figure 16: English Example - Whisper

Figure 17: Chinese Example - Whisper